Chapter 21 Single-Molecule Organic Electronics and Optoelectronics

Ling Zang, Xiaomei Yang, Tammene Naddo
The Laboratory for Nanoscale Exploration and Single-Molecule Imaging (NESMI), Department of Chemistry and Biochemistry, Southern Illinois University, Carbondale, IL 62901

Introduction to Organic Electronic and Optoelectronic Materials and Devices (Eds. Sun & Dalton) CRC Press, 2008. ISBN-10: 0849392845

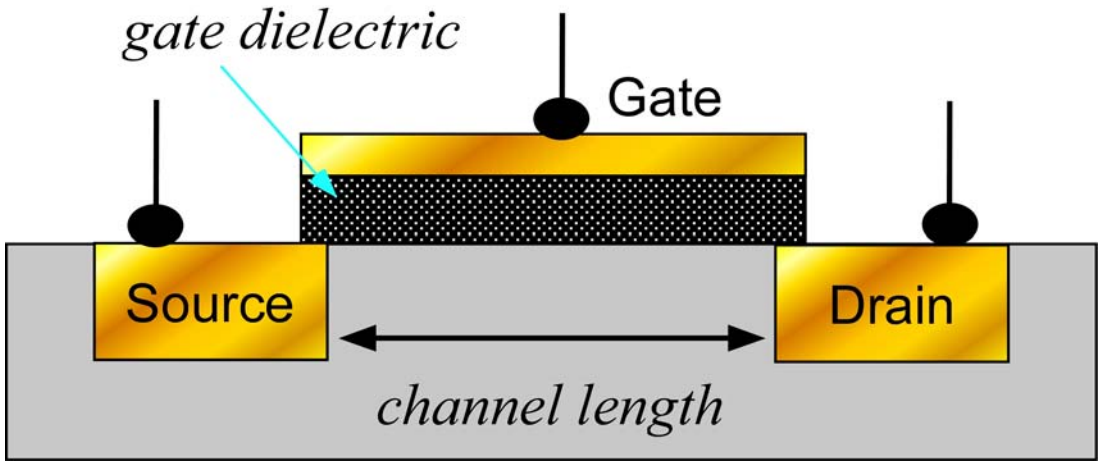

Figure 21.1. A schematic illustration of cross section of a lateral field-effect transistor (FET). Source electrode: providing the major charge carriers (e- for n-type semiconductor, h+ for p-type semiconductor); Drain electrode: drawing the major carriers from channel materials; Gate electrode: providing local electrical field to modulate the charge carrier density and mobility inside the channel material; Gate dielectric layer: functioning as an insulating layer between gate and channel material, and enabling creation of spatial gradient of the electrical field across the dielectric layer. Gate effect is dependent on both the electrical property and thickness of the dielectric layer.

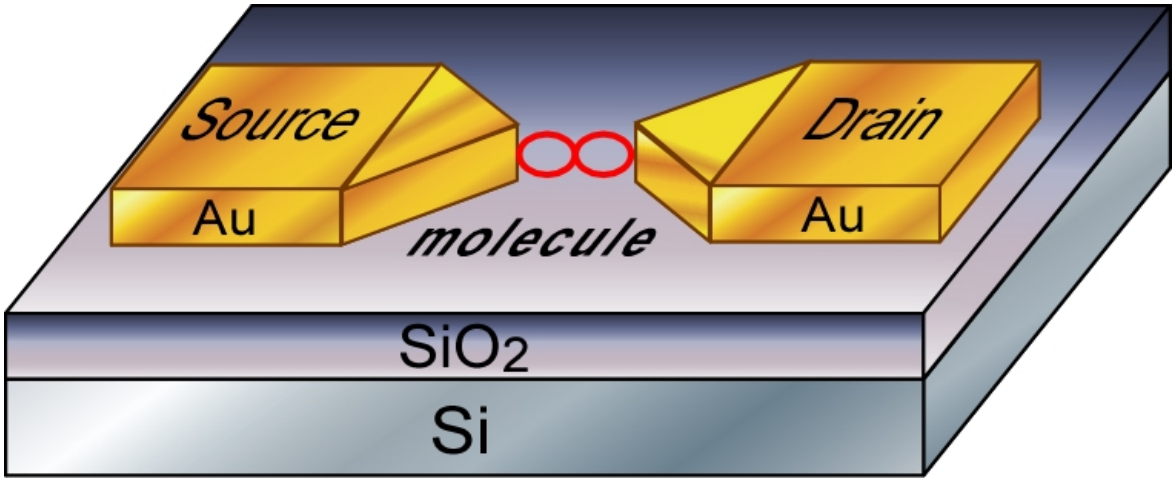

Figure 21.2. A nanoelectrode molecular junction fabricated on oxidized silicon surface, which can be adapted to be a FET device by attaching a gate to the silicon substrate.

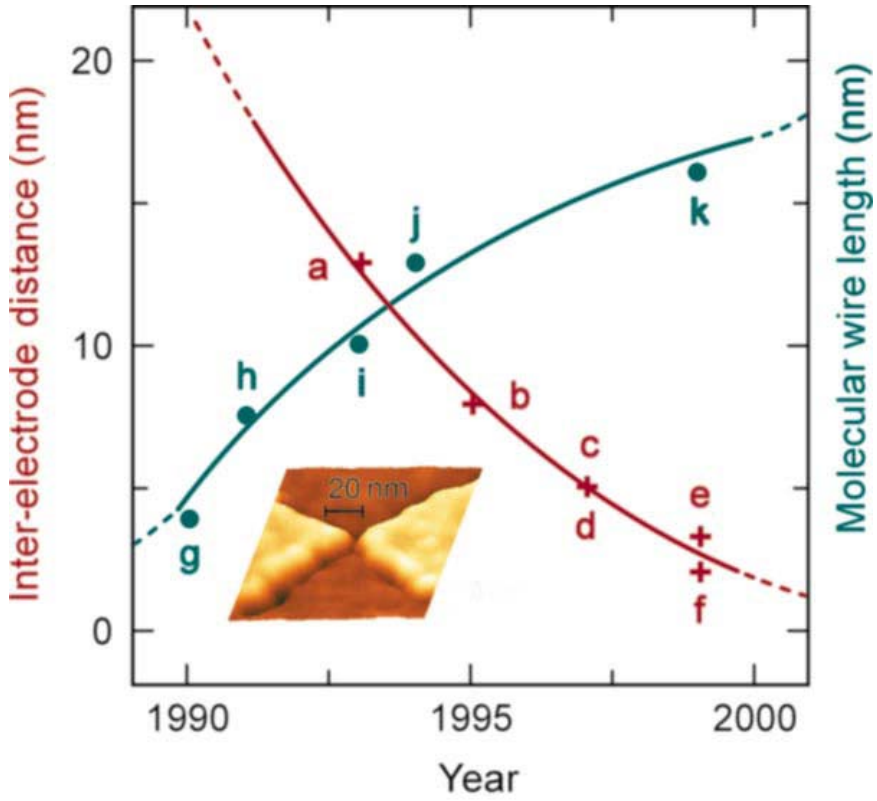

Figure 21.3. Red, inter-electrode distance; green, molecular wire length. **a**, **b**, Planar standard e-beam nanolithography nanojunctions. **b**, **e**, Co-planar e-beam nanojunctions with the electrode metal at the same height as the substrate. **d**, **f**, Suspended planar nanojunctions fabricated by electrodeposition (**d**) and electrochemistry (**f**). **g**, **h**, Long oligoimide molecular lines. **i**, Thiophene-ethynylene oligomers. **j**, Phenylalkyne oligomers. **k**, Alternating block co-oligomers of (1,4-phenylene ethynylene)s and (2,3-thiophene ethynylene)s. Inset, AFM tapping mode image of a 4-nm coplanar nanojunction. In **e**, the two gold-palladium metal electrodes are only 1 nm higher than the background silicon wafer surface. (Reprinted with permission from *Nature*, vol. 408, p541-8, 2000. Copyright 2000 Macmillan Magazines Ltd).

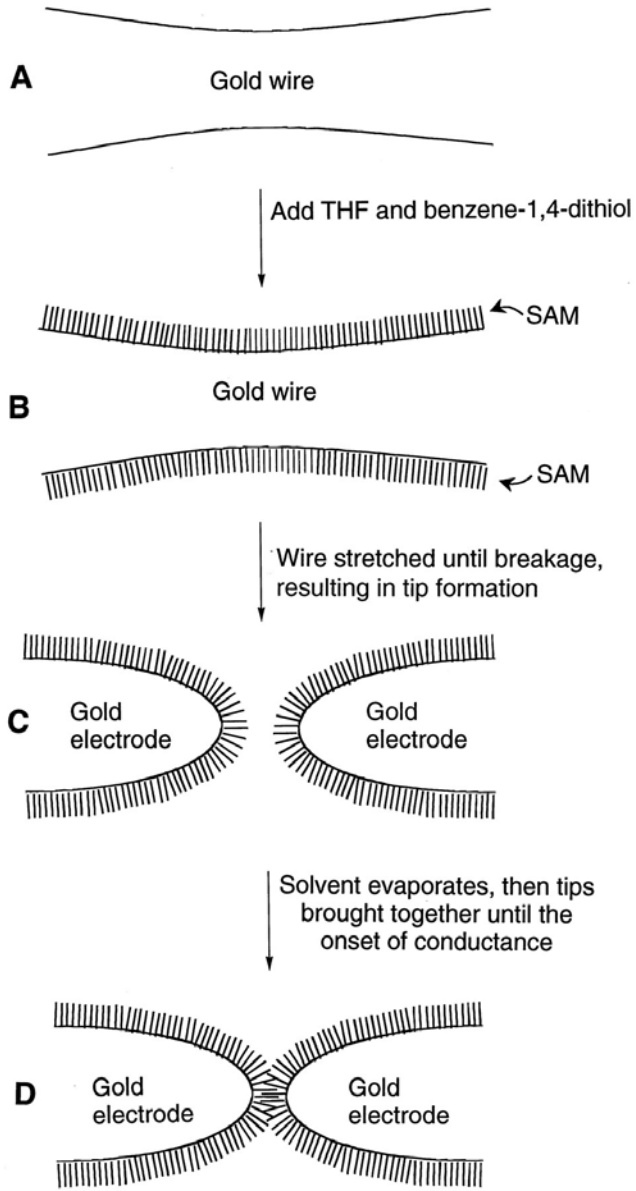

Figure 21.4. A schematic illustration of fabrication of Reed break-junction: (**A**) The gold wire of the break junction before breaking and tip formation. (**B**) After addition of benzene-1,4-dithiol, a self-assembled monolayer forms on the gold wire surfaces. (**C**) Mechanical breakage of the wire in solution produces two opposing gold contacts that are SAM-covered. (**D**) After the solvent is evaporated, the gold contacts are slowly moved together until the onset of conductance is achieved. A zoom-in view of the nanojunction (**D**) is presented in Figure 21.5. (Reprinted with permission from *Science*, vol. 278, p252-4, 1997. Copyright 1997 American Association for the Advancement of Science).

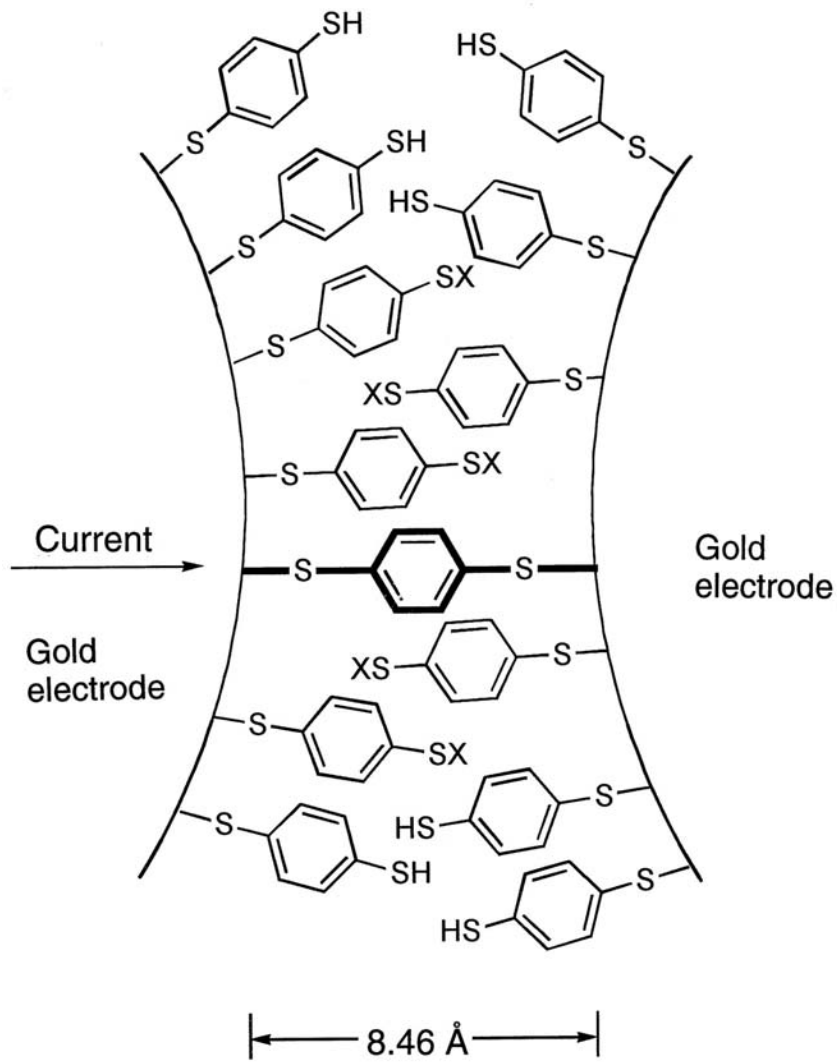

Figure 21.5. A schematic of a benzene-1,4-dithiolate SAM between two proximal gold electrodes. The thiolate is normally H-terminated after deposition; end groups denoted as X can be either H or Au, with the Au potentially arising from a previous contact/retraction event. These molecules remain nearly perpendicular to the Au surface, making other molecular orientations unlikely. (Reprinted with permission from *Science*, vol. 278, p252-4, 1997. Copyright 1997 American Association for the Advancement of Science).

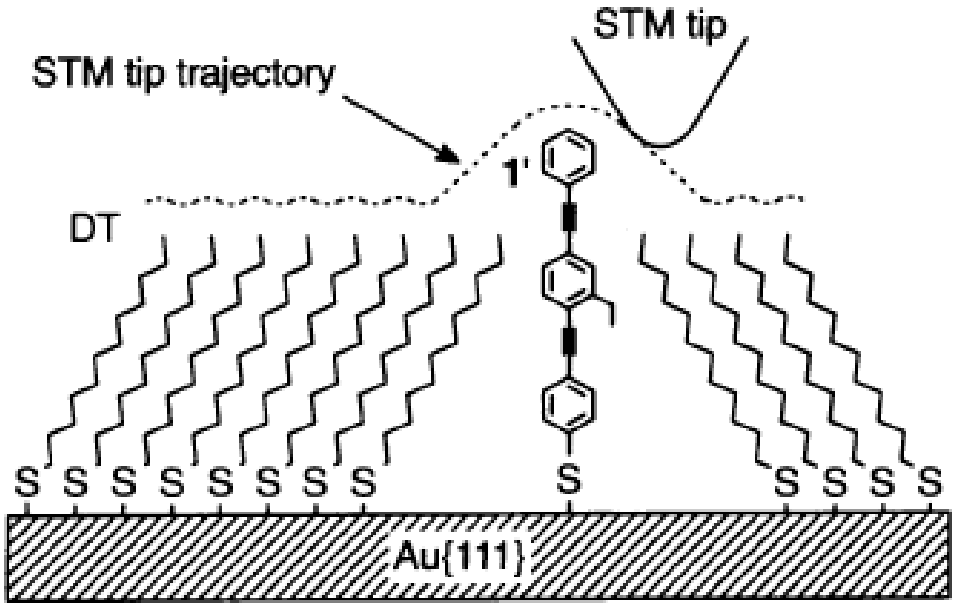

Figure 21.6. A schematic representation of a thiol-terminated conjugate molecule embedded in a alkyl-thiol monolayer Au {111}. The trajectory of the STM tip traces out a surface of constant current. The relatively flat monolayer can be imaged by an atomic scale asperity on the end of the STM tip with resolution of the molecular lattice. (Reprinted with permission from *Science*, vol. 271, p1705-7, 1996. Copyright 1996 American Association for the Advancement of Science).

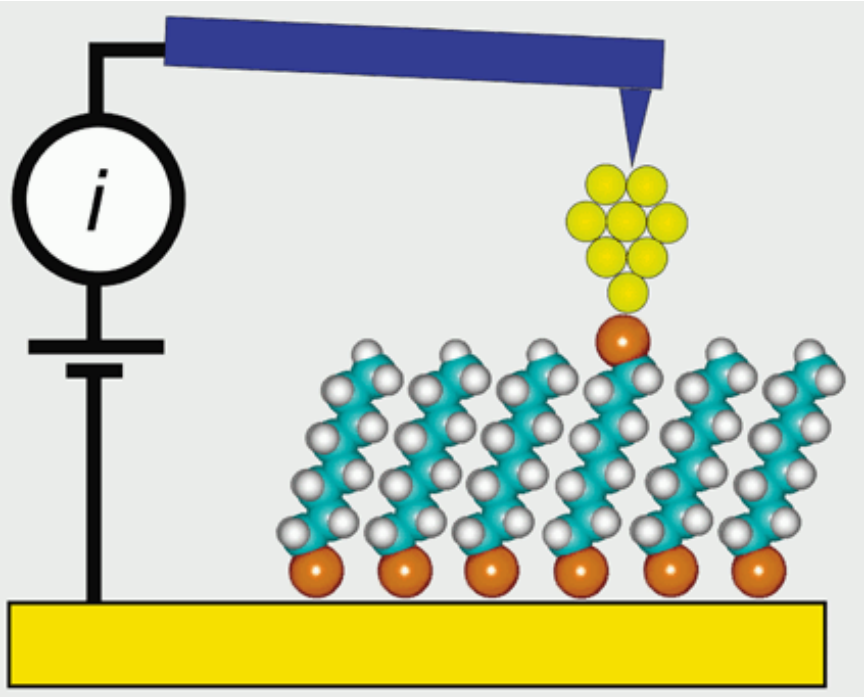

Figure 21.7. Molecular circuit: the conductivity of an isolated 1,8-octanedithiol molecule can be measured by chemically bonding one of its thiol moieties (orange) to a gold base electrode and the other thiol moiety to a gold nanoparticle that is in contact with the gold tip of a conducting atomic force microscope. (Reprinted with permission from *C&EN*, vol. 79, p14, 2001, Oct. 22. Copyright 2001 American Chemical Society).

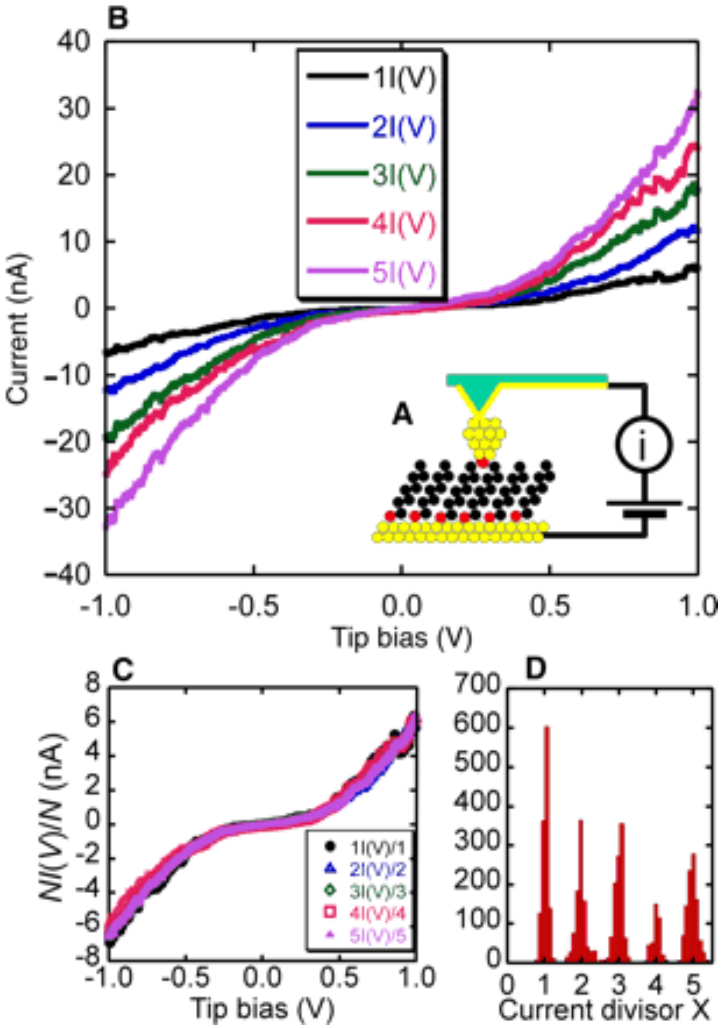

Figure 21.8. (**A**) Schematic representation of the AFM based measurement of single-molecule experiment. The sulfur atoms (red dots) of octanethiols bind to a sheet of gold atoms (yellow dots), and the octyl chains (black dots) form a monolayer. The second sulfur atom of a 1,8-octanedithiol molecule inserted into the monolayer binds to a gold nanoparticle, which in turn is contacted by the gold tip of the conducting AFM. (**B**) *I-V* curves measured with the apparatus diagrammed in (A). The five curves shown are representative of distinct families, *N(I-V)*, that are integer multiples of a fundamental curve, *I-V* (*N* = 1, 2, 3, 4, and 5). (**C**) Curves from (B) divided by 1, 2, 3, 4, and 5. (**D**) Histogram of values of a divisor, *X* (a continuous parameter), chosen to minimize the variance between any one curve and the fundamental curve, *I-V*. It is sharply peaked at integer values 1.00 ± 0.07 (1256 curves), 2.00 ± 0.14 (932 curves), 3.00 ± 0.10 (1002 curves), 4.00 ± 0.10 (396 curves) and 5.00 ± 0.13 (993 curves). (Spreads are ±1 SD.) Of 4579 randomly chosen curves, over 25% correspond to the *X* = 1 (single-molecule) peak. (Reprinted with permission from *Science*, vol. 294, p571-4, 2001. Copyright 2001 American Association for the Advancement of Science).

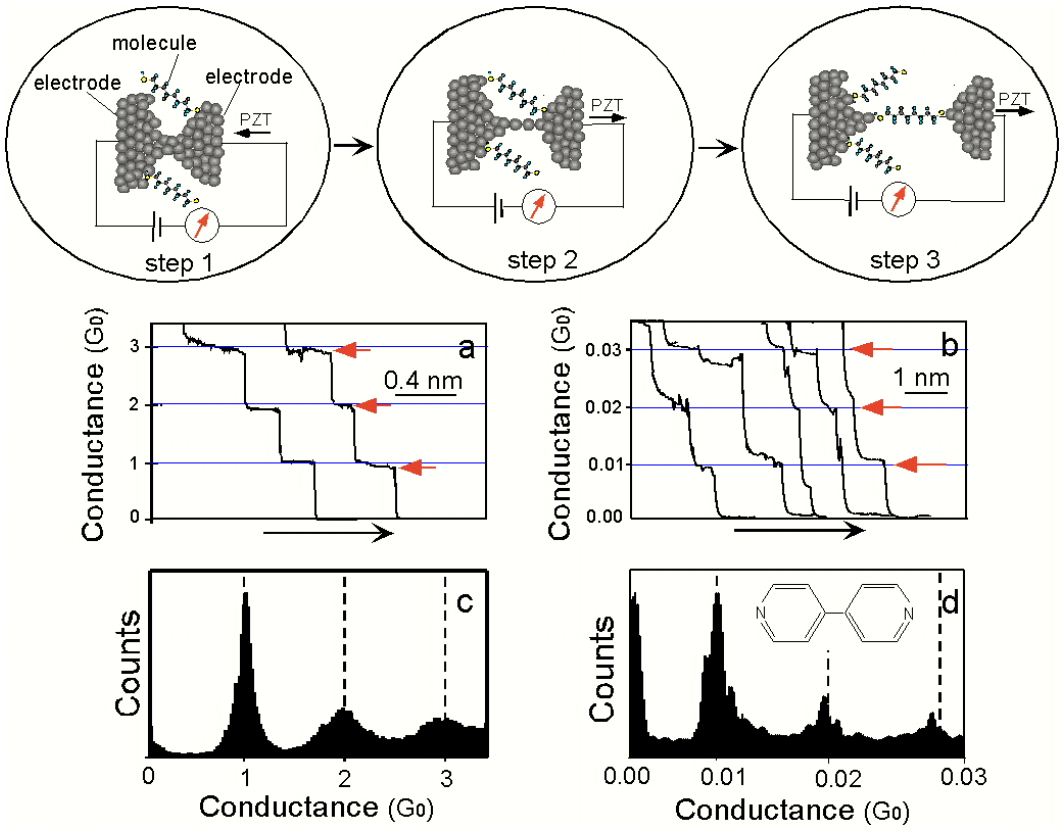

Figure 21.9. Measurement of single molecule conductance based on STM brek-junction technique. Step 1: A piezoelectric transducer (PZT) drives an electrode into contact with another electrode in a solution containing sample molecules. Step 2: The first electrode is then pulled back to form an atomic-scale neck between the two electrodes, which is signaled by conductance quantization (a,c). Step 3: After breaking the atomic-scale neck, the sample molecules start to bridge the two electrodes via chemical bonds. Further pulling breaks the individual molecules, which leads to a new series of steps in the conductance (b). Conductance histogram (d) constructed from a large number of measurements reveals well-defined peaks near integer multiples of a fundamental value (0.01G0 for 4,4'-bipyridine shown here), which is identified as the conductance of a single molecule. (Reprinted with permission from *Faraday Discuss.*, vol. 131, p111-120, 2006. Copyright 2006 Royal Chemical Society).

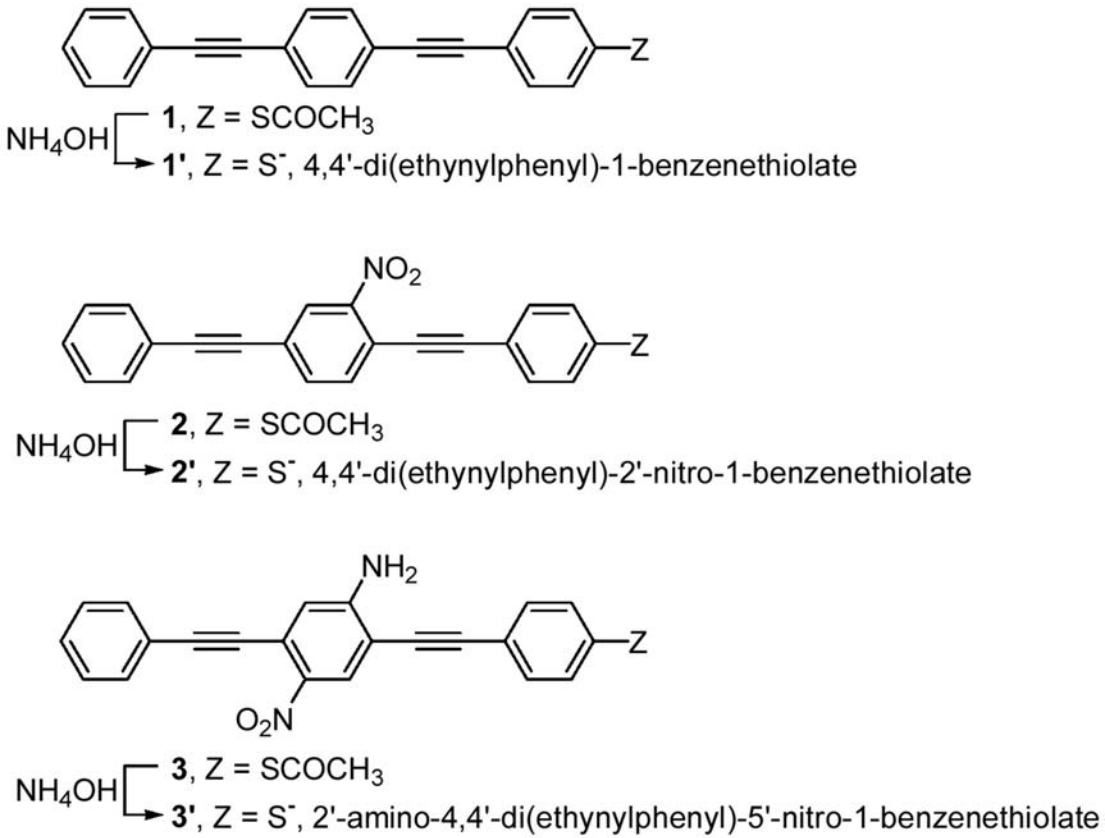

Figure 21.10. Molecules for which switching was observed (**1'**, **2'**, and **3'**) are produced in situ from the corresponding thioacetyls (**1**, **2**, and **3**, respectively) with the deprotection reaction shown for each. Aqueous ammonium hydroxide is used to hydrolyze the acetyl protecting group, generating the thiolate or thiol. The thiolate/thiol can then adsorb on the Au{111} surface, inserting at existing defect sites in the dodecanethiolate monolayer matrix. (Reprinted with permission from *Science*, vol. 292, p2303-7, 2001. Copyright 2001 American Association for the Advancement of Science).

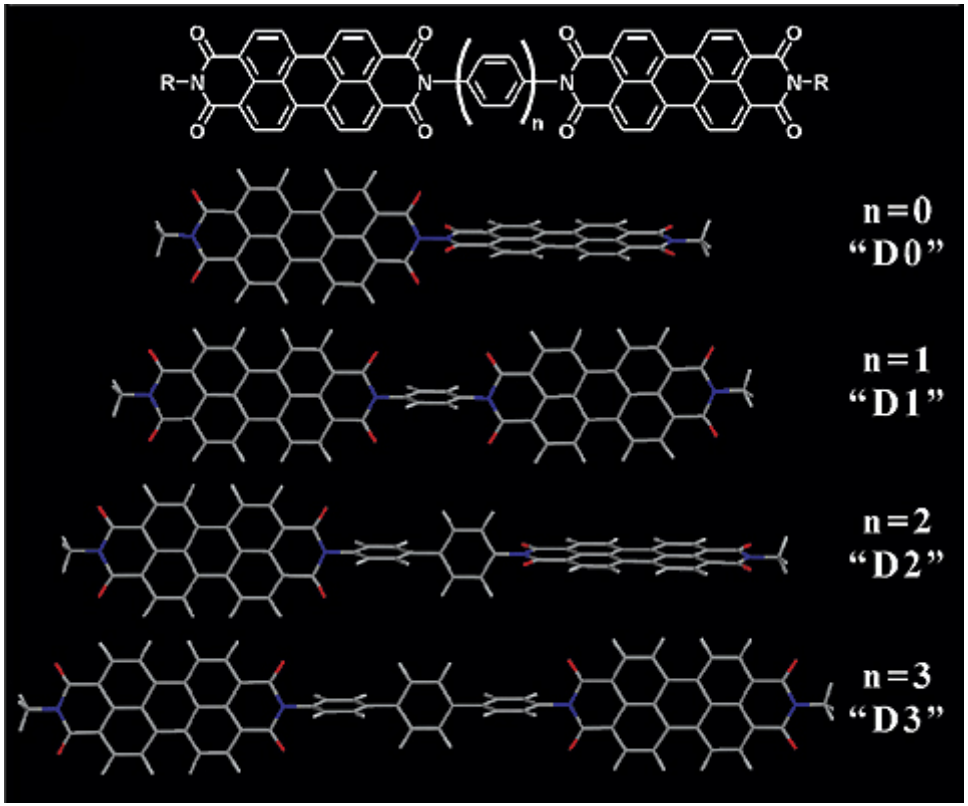

Figure 21.11. Structures of PTCDI dimers (**P-P**): **D0**, **D1**, **D2**, and **D3**, and monomer **M**. Side-chain R = nonyldecyl. The dimers can potentially be used as molecular wires by changing the side-chains to thiol moieties. PTCDI stands for perylene tetracarboxylic diimide. (Reprinted with permission from *J. Am. Chem. Soc.*, vol. 126, p16126-33, 2002. Copyright 2002 American Chemical Society).

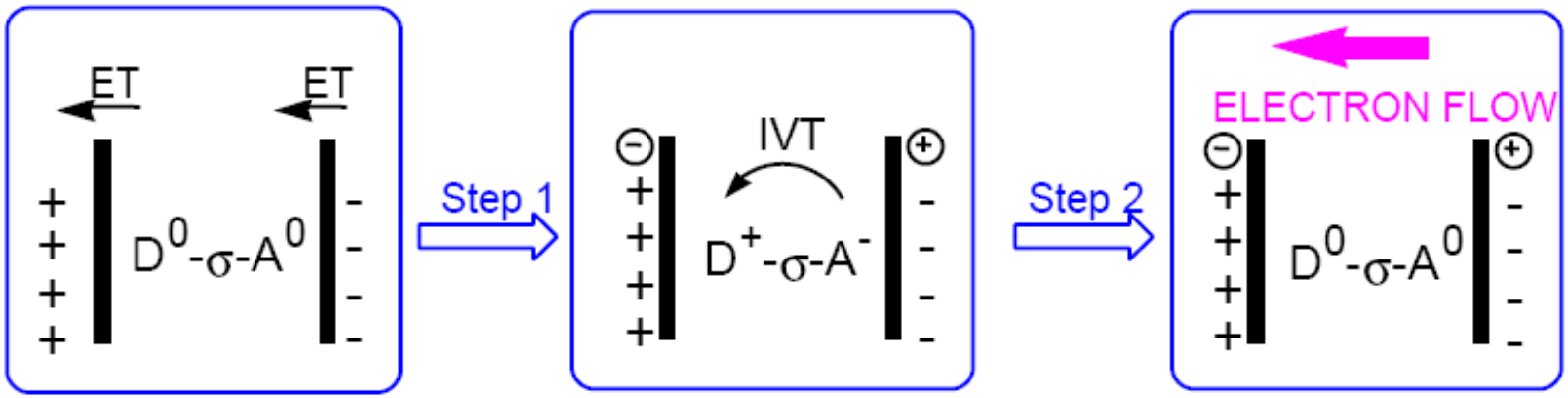

Figure 21.12. Schematic picture of the Aviram–Ratner diode involving a D–s–A molecule and two metallic electrodes, where D stands for electron donor, and A for acceptor. The electron flow is favored for the forward process as marked by the red arrow: at first electrons move from the cathode to the acceptor and from the donor to the anode. Then, molecules recover the ground state via an intervalence transfer (IVT). To make it rectifying, the reverse bias process (involving auto-ionization) must be infrequent. (Adapted from Robert Metzger presentation at the Workshop "Advances in Molecular Electronics: from molecular materials to single molecule devices", February 23 - 27, 2004, MPIPKS Dresden, Dresden, Germany; online: http://www.mpipks-dresden.mpg.de/~admol/)

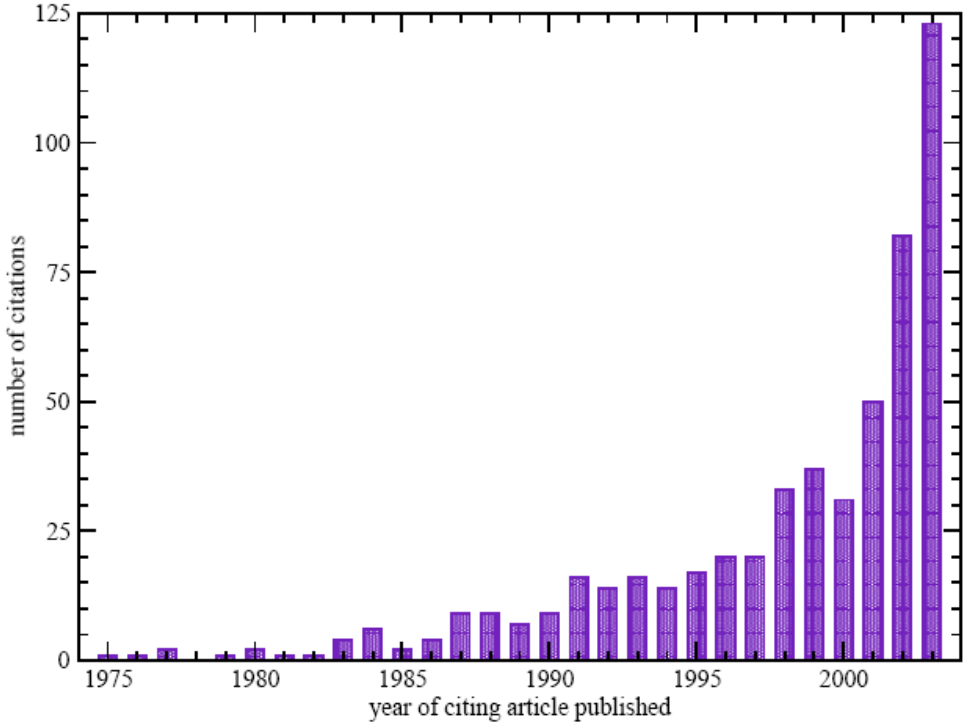

Fig. 13. Emerging of the field of molecular electronics and the increasing interest is indicated by the exponential increase in the number of annual citations to the seminal Aviram-Ratner study (*Chem. Phys. Lett.* 1974, 29, p277-283) during the last three decades. Data taken from the ISI Web of Knowledge.

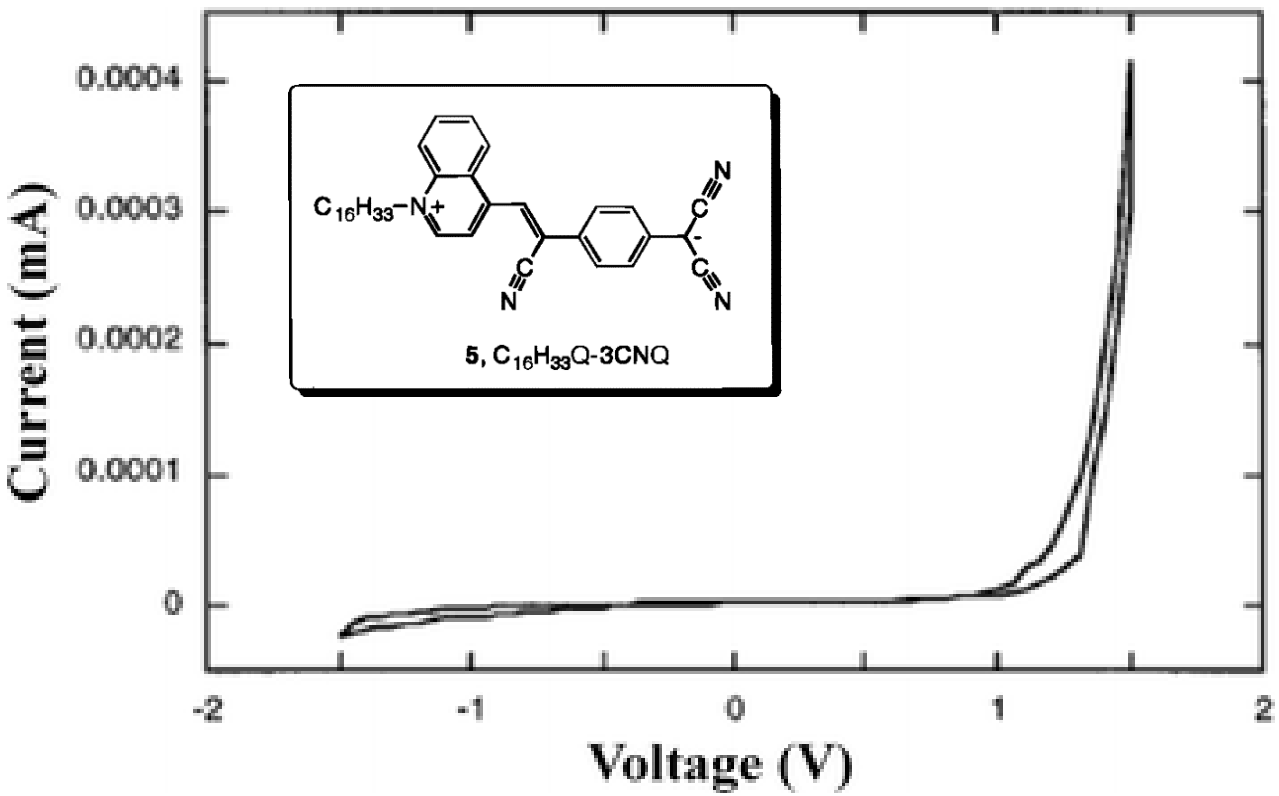

Figure 21.14. Current–voltage characteristic of the device comprising a monolayer of hexadecylquinolinium tricyanoquinodimethanide (inset) exhibits a very high rectification (rectification ratio around 26). [Reprinted with permission from *J. Am. Chem. Soc.*, 1997, 119, 10455–10466, Copyright 1997 American Chemical Society]

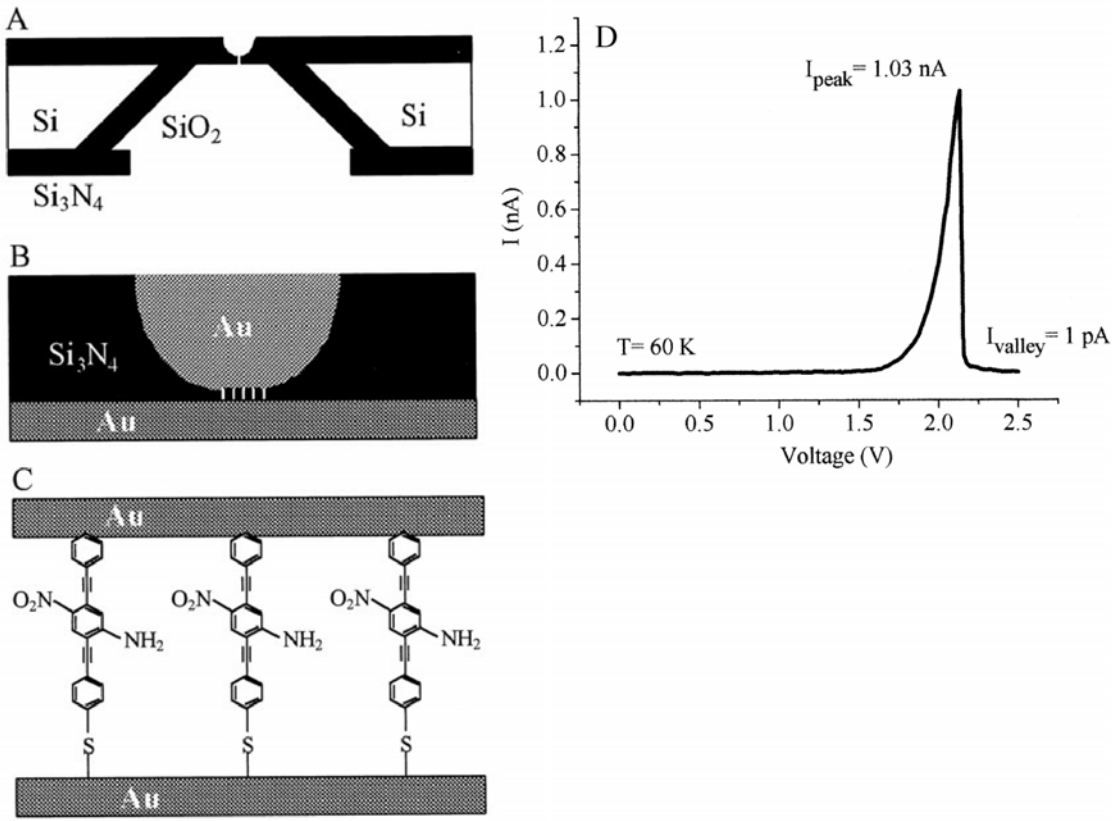

Figure 21.15. (A) Cross section of a silicon wafer with a nanopore etched through a suspended silicon nitride membrane. (B) Au-SAM-Au junction in the pore area. (C) Blowup of (B) with the channel molecules sandwiched in the junction. (D) I-V characteristics of the molecule (shown in C) at 60 K. The peak current density is ~50 A/cm2, the NDR is ~400 µohm · cm2, and the PVR is 1030:1. (Reprinted with permission from *Science*, vol. 286, p1550-2, 1999. Copyright 1999 American Association for the Advancement of Science).

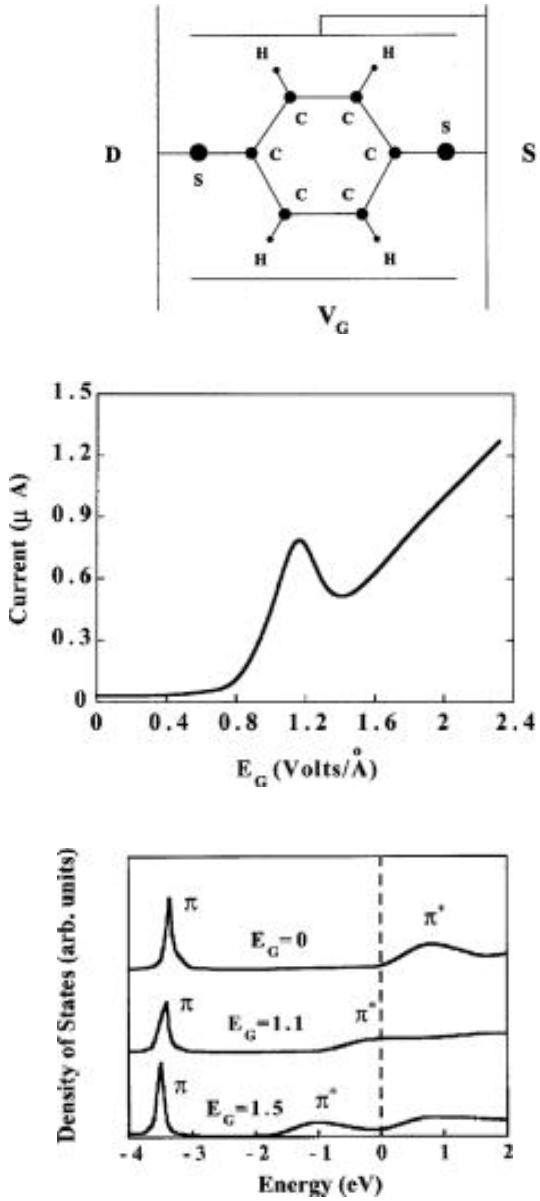

Figure 21.16. (top) Scheme of the three-terminal geometry used in the present study. The molecule is sandwiched between source and drain electrodes along the direction of electronic transport. The gate electrodes are placed perpendicular to the molecule plane. The Fermi level on one gate disk equals the source Fermi level while the other electrode is at a higher potential *VG* . (middle) Conductance of the molecule of Fig. 1 as a function of the external gate field. The source–drain bias is 0.01 V. (bottom) Difference between the density of states of the two semi-infinite electrodes with and without the benzene-1,4-dithiolate molecule in between, for three different gate fields *EG* (in units of V/Å). The left Fermi level has been chosen as the zero of energy. The right Fermi level is at 10 mV. (Reprinted with permission from *Appl. Phys. Lett.*, vol. 76, p3448, 2000. Copyright 2000 American Institute of Physics).

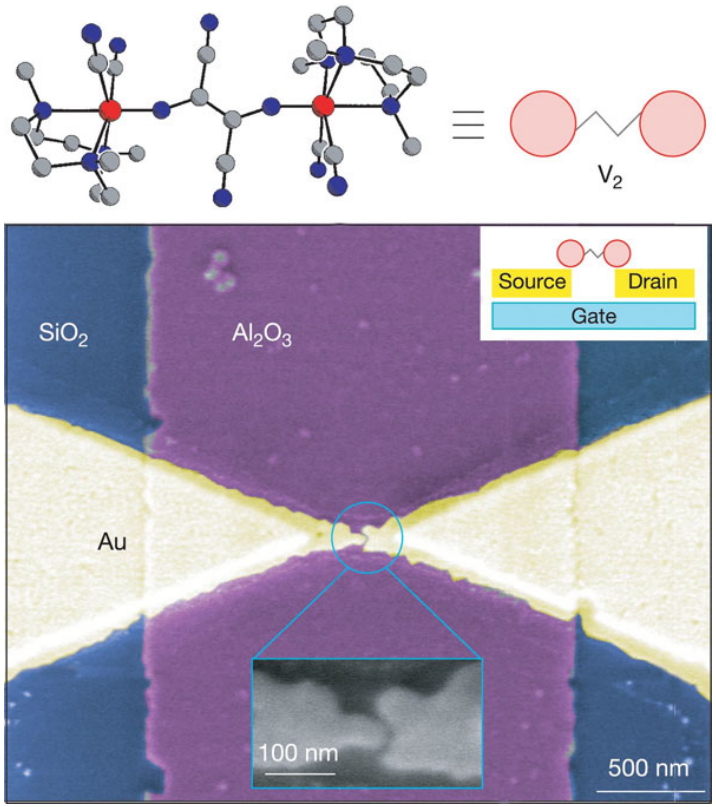

Figure 21.17. Fabrication of a single-molecule transistor incorporating a divanadium molecules. Top left, the structure of [(N,N',N''-trimethyl-1,4,7-triazacyclononane)2V2(CN)4(m-C4N4)] (the V2 molecule) as determined by X-ray crystallography; red, grey and blue spheres represent respectively V, C and N atoms. Top right, the schematic representation of this molecule. Main panel, SEM image (false color) of the metallic electrodes fabricated by electron beam lithography and the electromigration-induced break-junction technique. The image shows two gold electrodes separated by ~ 1 nm above an aluminum pad, which is covered with an ~ 3 nm thick layer of aluminum oxide. The whole structure was defined on a silicon wafer. The bright yellow regions correspond to a gold bridge with a thickness of 15 nm and a minimum lateral size of ~ 100 nm. The paler yellow regions represent portions of the gold electrodes with a thickness of ~ 100 nm. Main panel inset, schematic diagram of a single-V2 transistor. (Reprinted with permission from *Nature*, vol. 417, p725-9, 2002. Copyright 2002 Macmillan Magazines Ltd).

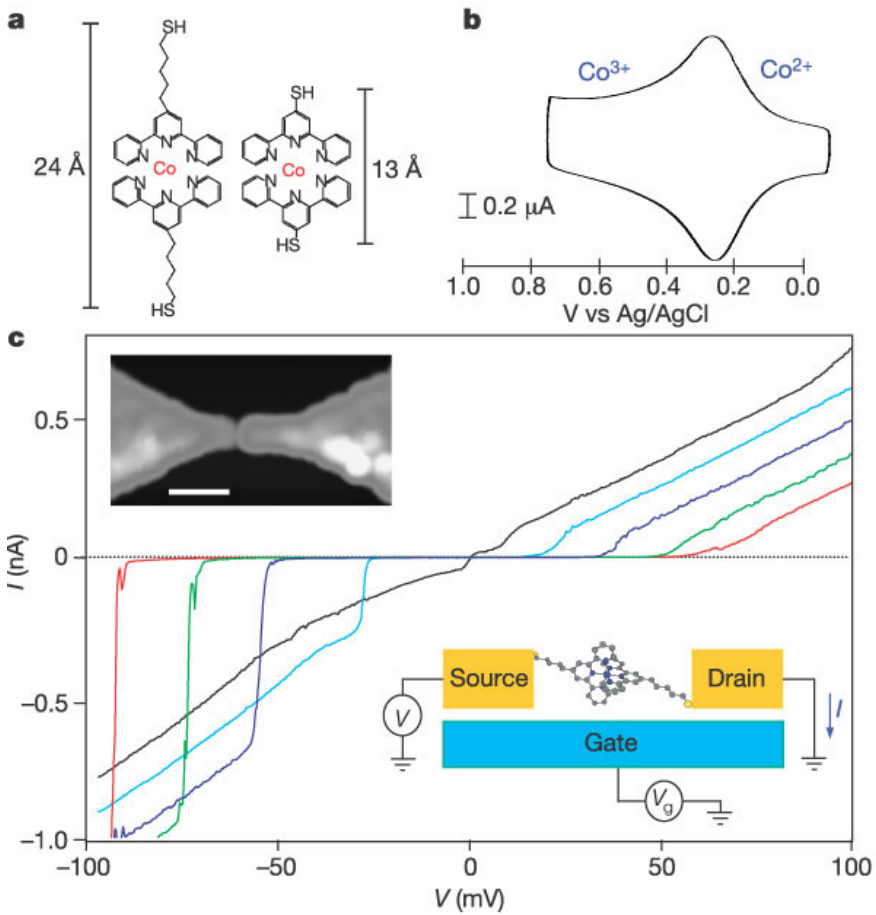

Figure 21.18. a) structure of the two molecules employed in the FET device. The scale bars show the lengths of the molecules as calculated by energy minimization. b) Cyclic voltammogram of the molecule with short linker in 0.1M tetra-n-butylammoniumhexafluorophosphate, acetonitrile showing the Co2+/Co3+ redox peak. c) I –V curves of a single-electron FET of the molecule with long linker at different gate voltages (Vg) from -0.4 V (red) to -1.0 V (black) with DVg ~ - 0.15 V. Upper inset, a topographic AFM image of the electrodes with a gap (scale bar, 100 nm). Lower inset, a schematic diagram of the device. (Reprinted with permission from *Nature*, vol. 417, p722-5, 2002. Copyright 2002 Macmillan Magazines Ltd).

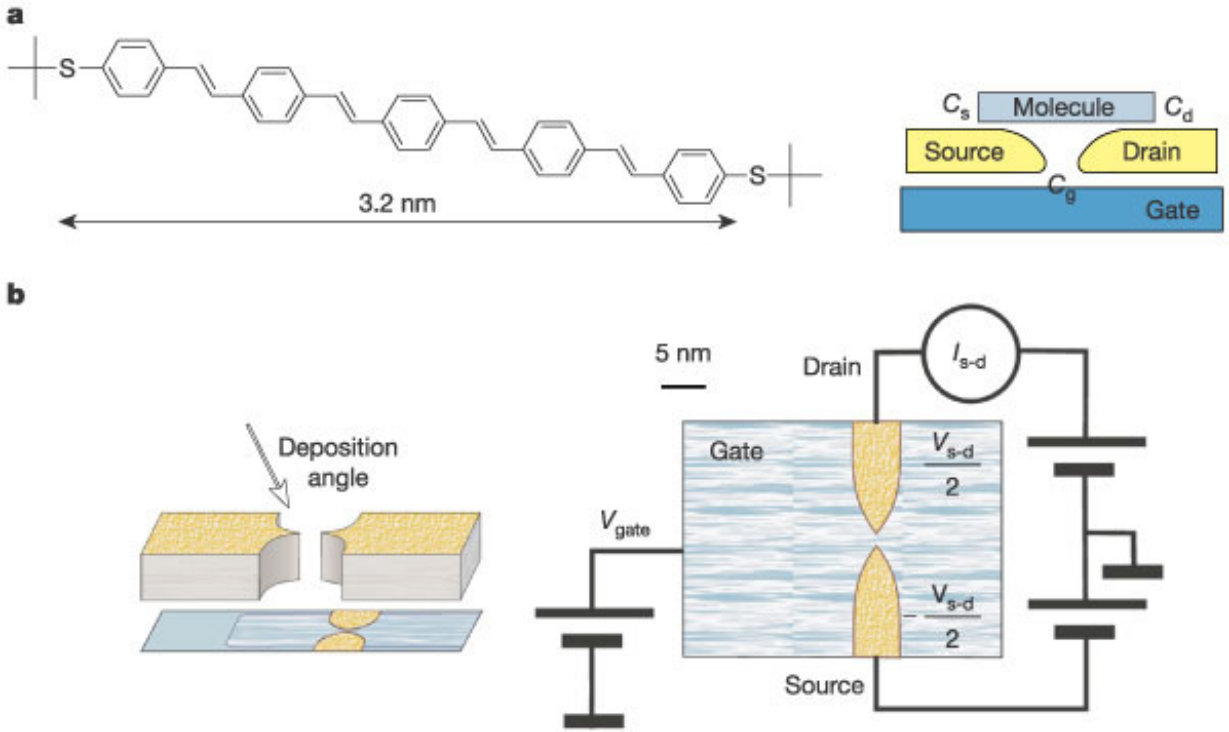

Figure 21.19. a) Molecular structure of OPV5 and schematic experimental set-up of the single-molecule FET fabricated with OPV5. b) Schematic representation of the device preparation procedure. (Reprinted with permission from *Nature,* vol. 425, p698-701, 2003. Copyright 2003 Macmillan Magazines Ltd).

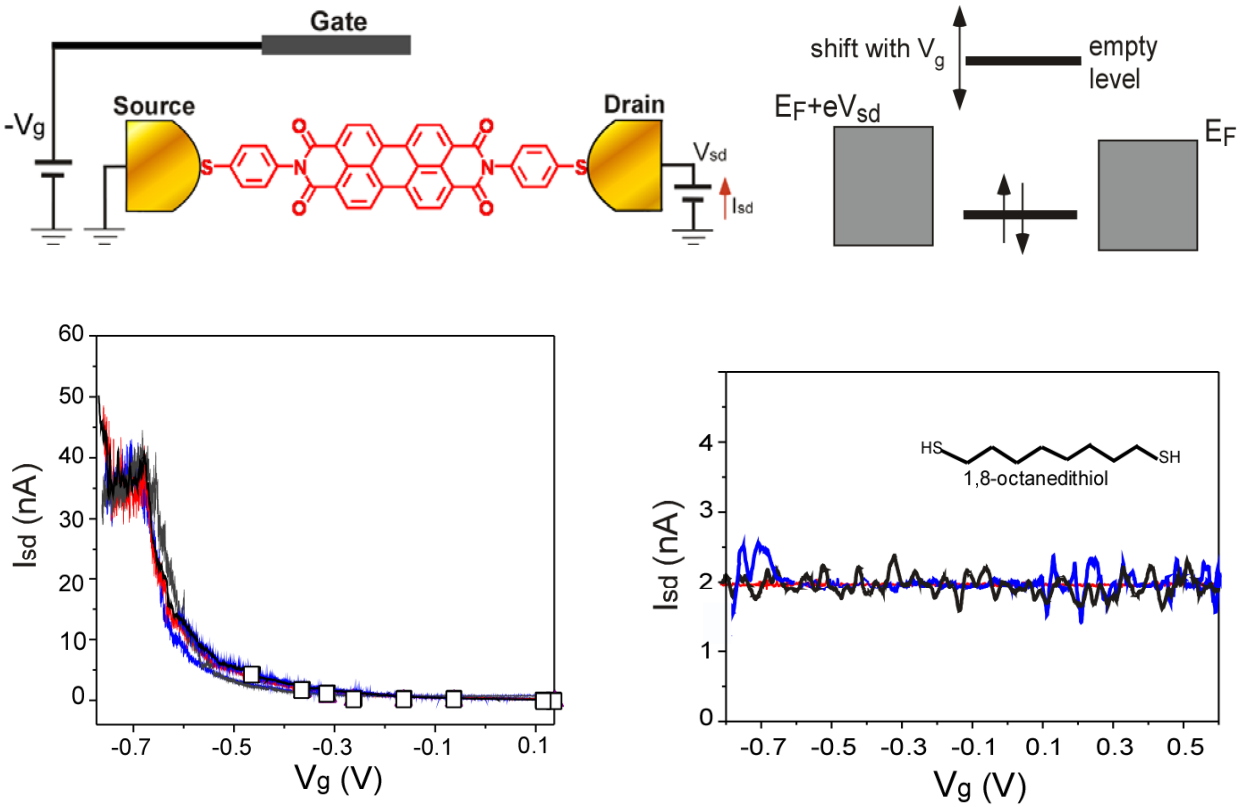

Figure 21.20. (top left) Schematic of a single molecule FET comprising a PTCDI molecule. An electrochemical electrode (Ag wire reference electrode in 0.1 M NaClO4) was used as gate. The gate and the source-drain bias voltages are controlled with a bipotentiostat (a Pt counter electrode not shown for clarity). (top right) The energy diagram of the gold-PTCDI-gold junction. (bottom left) Source-drain current (*I*sd) versus gate voltage (*V*g) for the single PTCDI FET. (bottom right) Control experiment on an alkanedithiol shows no gate voltage dependence. (Reprinted with permission from *J. Am. Chem. Soc.*, vol. 127, p2386-7, 2005. Copyright 2005 American Chemical Society).

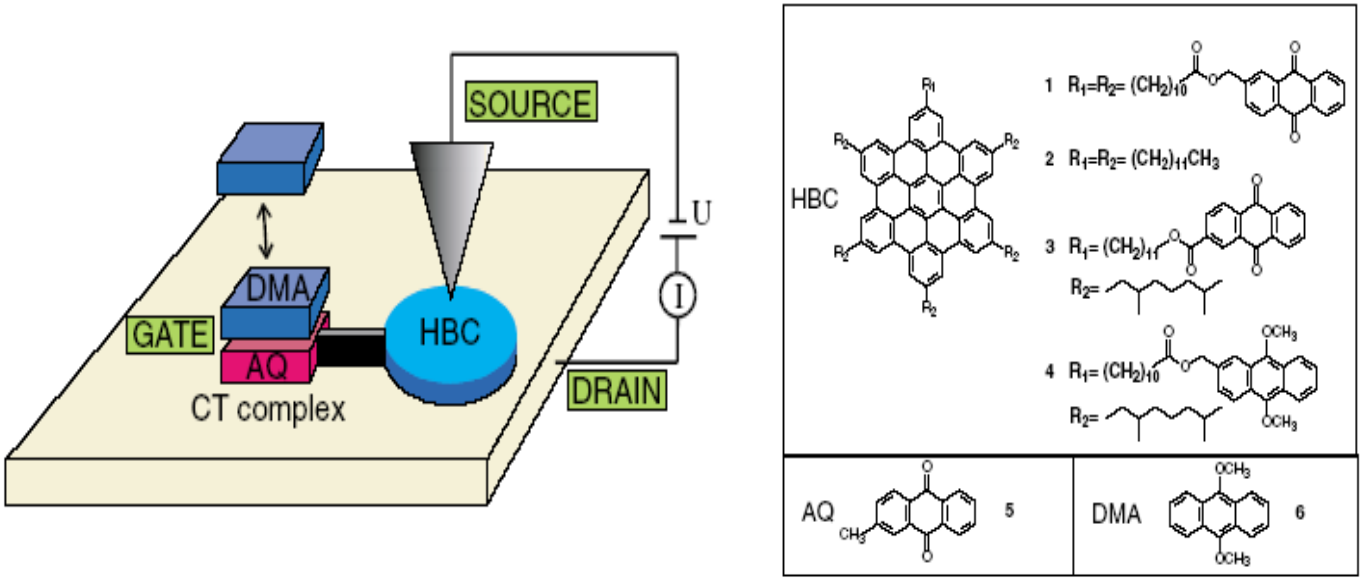

Figure 21.21. (left) Schematic of a prototype single-molecule chemical-field-effect transistor (CFET). (right) Chemical structures of the employed molecules: hexa*peri*-hexabenzocoronene (HBC) decorated with six anthraquinone (AQ) functions (1), hexaalkyl-HBC (2), HBC bearing either one AQ (3) or one 9,10-dimethoxyanthracene (DMA) function (4), methyl-AQ (5), and DMA (6). (Reprinted with permission from *Phys. Rev. Lett.*, vol. 92, p188303, 2004. Copyright 2004 American Physical Society).

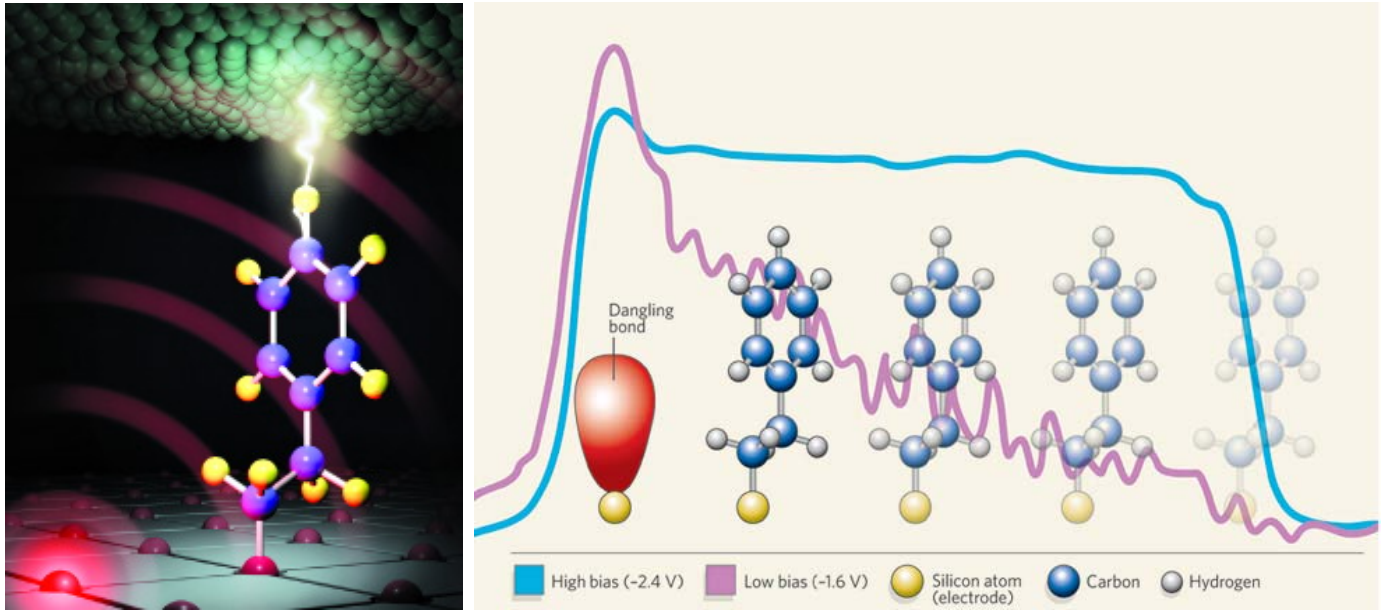

Figure 21.22. (left) A cartoon showing that the electric field from a surface ion (glowing red) can be used to regulate electrical conductivity between a nearby molecule and a scanning tunneling microscope tip (green). (right) The polymerization of a molecule (here an organic styrene-derived molecule, not to scale) on a silicon substrate stops abruptly at a dangling-bond site. The blue and purple lines indicate the height of the molecules, as seen by a scanning tunnelling microscope (STM) — a measure of the charge transport across the molecules. At higher bias (blue line), all molecules are 'turned on', and appear bright in the STM picture. At lower bias (purple line), all molecules should appear dark. The electrostatic potential of the negatively charged dangling bond causes the nearest molecules to remain bright. This suggests that such structures could be used to manipulate charge transport through molecular junctions. (Reprinted with permission from *Nature*, vol. 435, p575-7, 2005. Copyright 2005 Macmillan Magazines Ltd; and *C&EN*, vol. 83, p7, 2005, June 6. Copyright 2005 American Chemical Society).

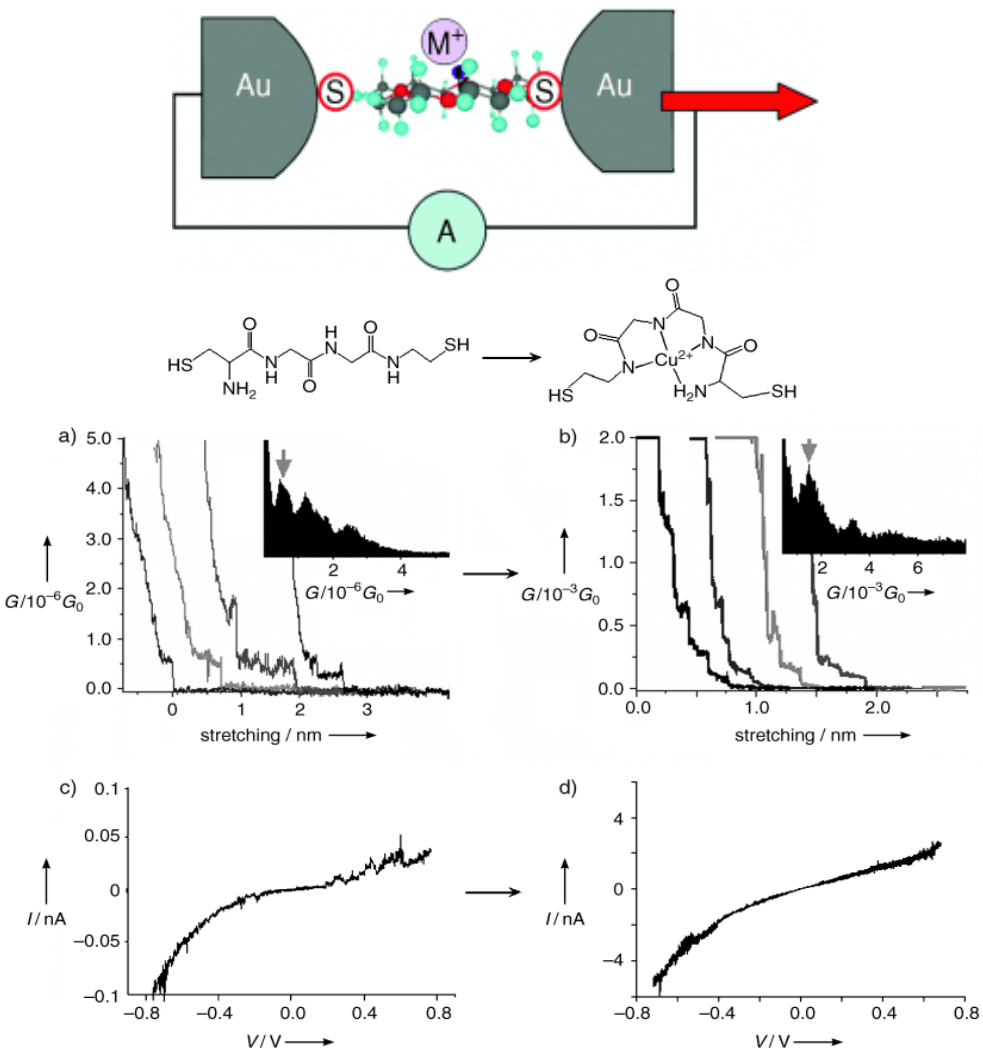

Figure 21.23. (top) Schematic illustration of a molecular junction formed by the separation of two electrodes (PZT=piezoelectric transducer). (bottom) Individual conductance curves of a peptide, Cysteamine-Gly-Gly-Cys. a) before and b) after binding to Cu2+; the insets show the conductance histograms. I–V curves of the same peptide c) before and d) after binding to Cu2+. (Reprinted with permission from *Angewandte. Chem., Intl.*, vol. 43, p6148-52, 2004. Copyright 2004 Wiley-VCH Verlag GmbH & Co. KGaA, Weinheim).

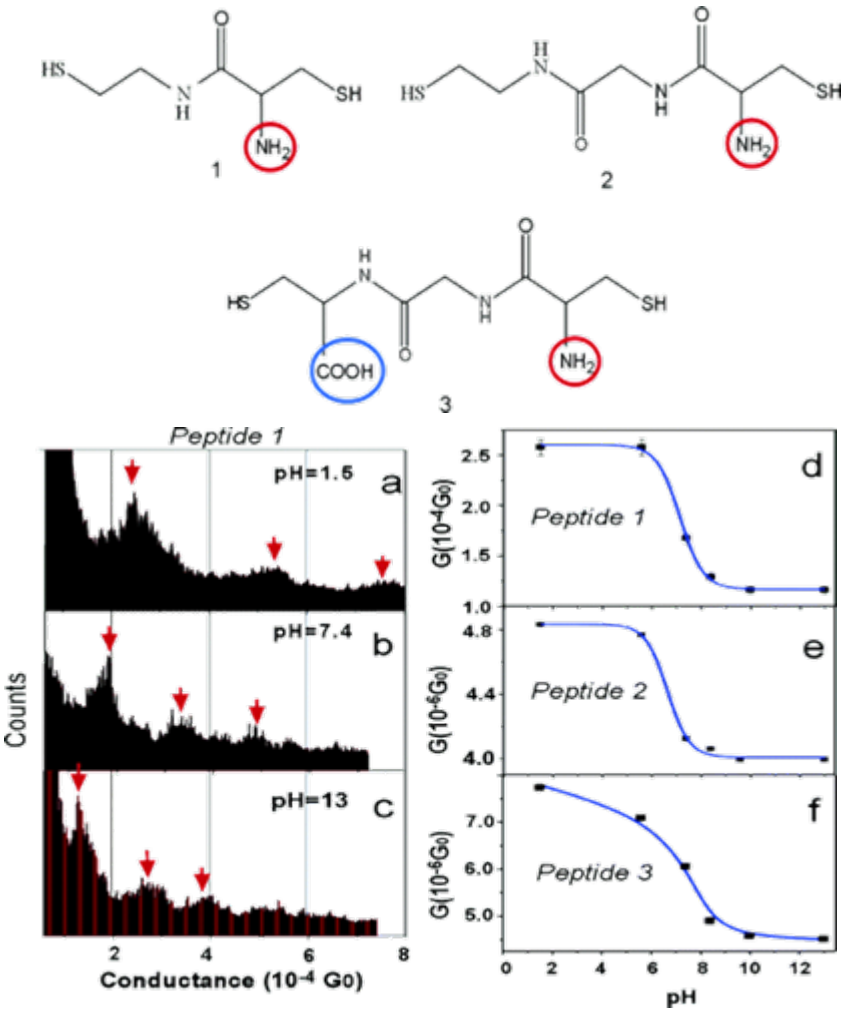

Figure 21.24. (top panel) Three peptides used in the pH titration. (a-c) Conductance histograms of peptide 1 obtained at various pH. Conductance vs pH for peptides 1 (d), 2 (e), and 3 (f). The solid lines show the sigmoidal fitting. (Reprinted with permission from *J. Am. Chem. Soc.*, vol. 126, p5370-1, 2005. Copyright 2005 American Chemical Society).

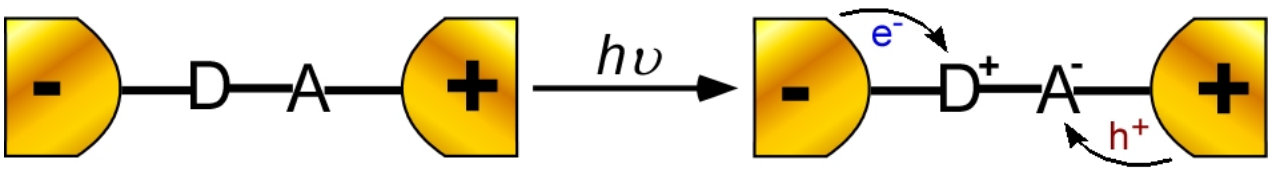

Figure 21.25. A photodiode comprising a donor-acceptor (D-A) molecule bridged between two metal electrodes (with donor linked to the cathode and acceptor to the anode). In the absence of illumination, the molecule is not favorable for electron transport due to the high energy barrier at the molecule/metal interface, i.e., donor is hard to be reduced and acceptor is hard to be oxidized. Upon illumination on either D or A, intramolecular electron transfer can be initiated by the increased energy at the excited state. If the lifetime of the charge separation state thus created is long enough, subsequent charge injection from the electrodes will neutralize the ionic radicals and recover the D-A molecule, enabling electrical current flowing through the molecular junction --- a prototype *single-molecule photodiode*. Theoretically, the illumination intensity (number of photons) can be counted by measuring the electrical current (number of the electrons flowing through). Note: the alignment of molecular junction is reverse in direction to the case of Avriam-Ratner molecular diode (Figure 21.12), where no optical excitation is applied.

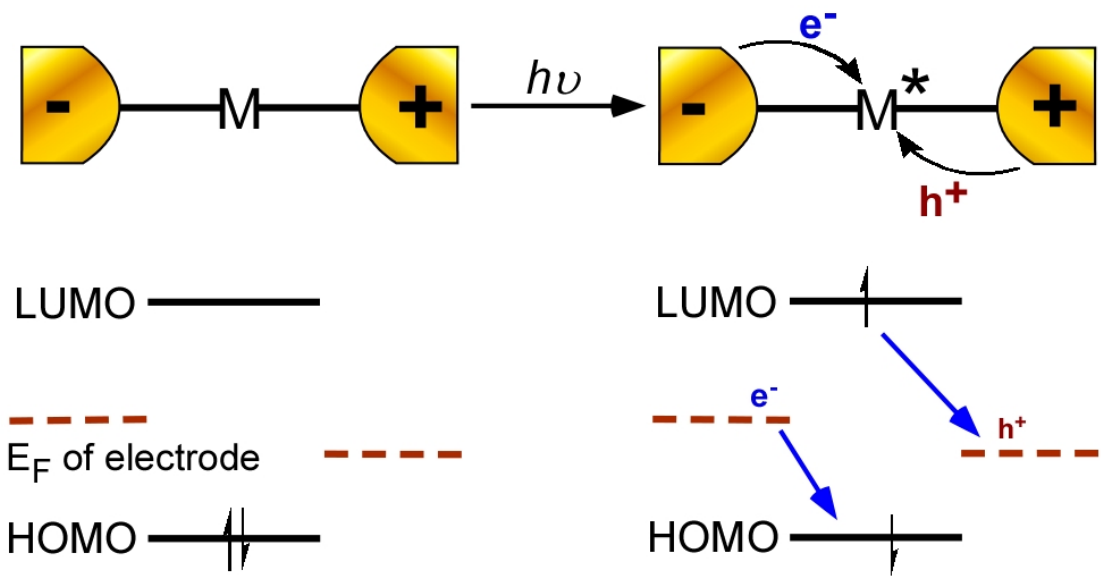

Figure 21.26. A phototransistor comprising a molecule (M) bridged between two metal electrodes. In the absence of illumination, the molecule is not favorable for electron transport due to the high energy barrier at the molecule/metal interface, i.e., the molecule is neither easy to be reduced nor to be oxidized at moderate bias. Upon illumination, the molecule gets excited and thus possesses higher energy at the excited state, making it more powerful for both donating and accepting an electron. Whichever occurs the first, the molecule will be charged via interfacial charge trasnfer, followed by neutralization by charge injection from the other electrode, thus enabling electrical current flowing through the molecular junction. If consider the optical modulation in analog to the electrical field effect in the conventional FET, the optoelectronic molecular junction shown in this figure acts as a *phototransistor*, for which the 'gate' is the optical excitation.

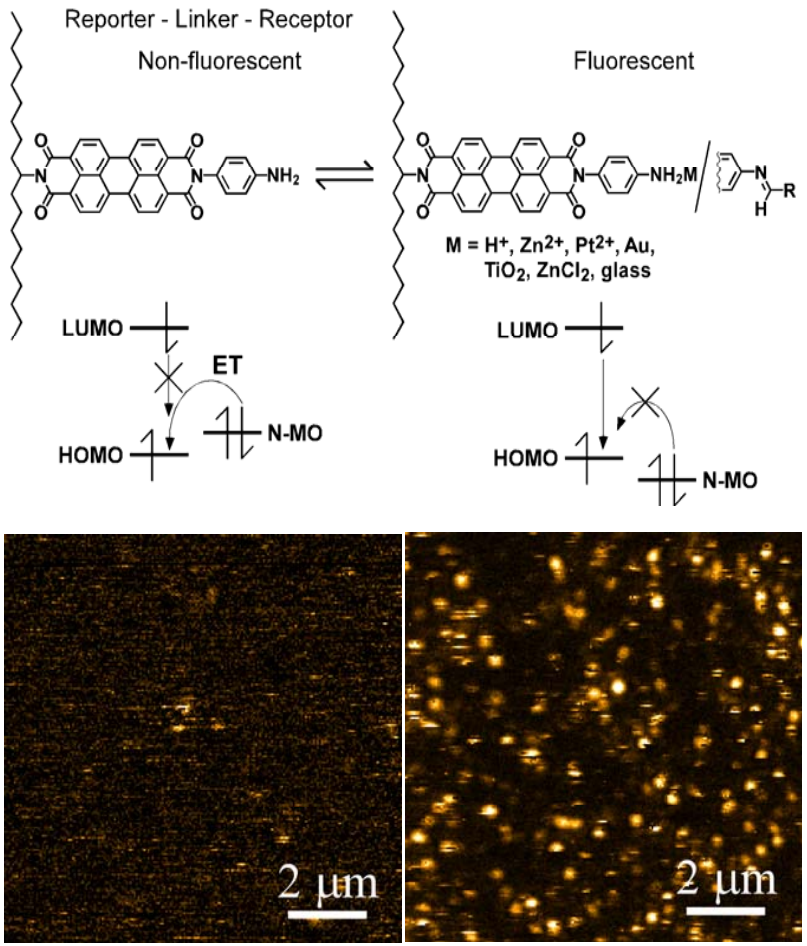

Figure 21.27. (top panel) A molecular orbital diagram for the free single-molecule probe illustrates how intramolecular electron transfer from a nonbonding electron pair (N–MO) to the highest occupied molecular orbital (HOMO) prevents fluorescence. Once the molecule binds to metal ions or proton, the N–MO drops in energy, and the intramolecular electron transfer gets blocked, turning on the fluorescence, which occurs with excited electrons going from the lowest unoccupied molecular orbital (LUMO) to the HOMO. (bottom panel) Single molecule fluorescence images of the molecule spin-coated onto quartz (left) and glass (right) surface, measured by scanning confocal microscopy. The glass (from Corning) contains dopant transition metal ions such as Ti(IV), Zn(II), which can be bound to the amine moiety of the molecule. (Reprinted with permission from *J. Am. Chem. Soc.*, vol. 124 p10640-1, 2002. Copyright 2002 American Chemical Society).

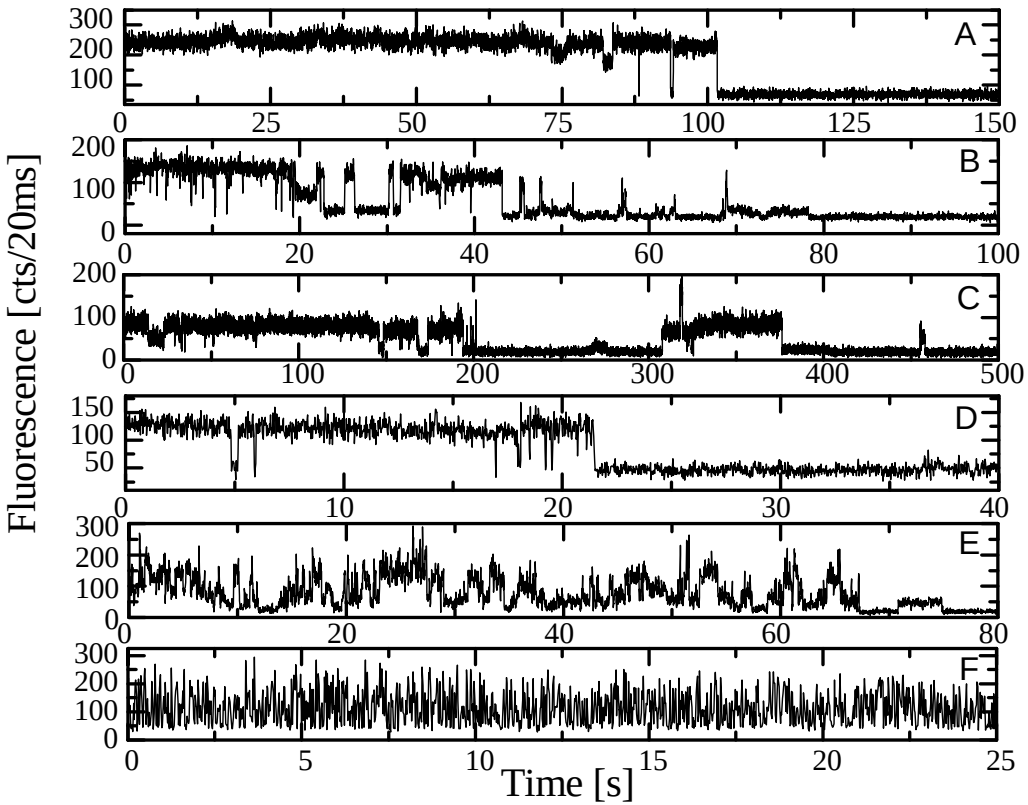

Figure 21.28. Characteristic single molecule fluorescence time trajectories for the single-molecule sensor (shown in Figure 21.27) applied in different sample systems: (A) in a PVB 30 nm thin film, (B) and (C) on glass, (D) on quartz following exposure to dioxane/HCl vapor., (E) and (F) on quartz after several days (no initial fluorescence observed). (Reprinted with permission from *J. Am. Chem. Soc.*, vol. 124 p10640-1, 2002. Copyright 2002 American Chemical Society).